Chaos, entanglement, and decoherence in the quantum kicked top

Shohini Ghose,[1] Rene Stock,[2] Poul Jessen,[3] Roshan Lal,[1,4] and Andrew Silberfarb[5]
[1]*Department of Physics and Computer Science, Wilfrid Laurier University, Waterloo, Ontario, Canada N2L 3C5*
[2]*Department of Physics and Astronomy, University of Toronto, Ontario, Canada M5S 3H8*
[3]*College of Optical Sciences, University of Arizona, Tucson, Arizona 85721, USA*
[4]*Indian Institute of Technology, Kharagpur-721 302, India*
[5]*Physical Measurement and Control, Edward L. Ginzton Laboratory, Stanford University, Palo Alto, California 94305, USA*
(Received 29 April 2008; published 20 October 2008)

We analyze the interplay of chaos, entanglement, and decoherence in a system of qubits whose collective behavior is that of a quantum kicked top. The dynamical entanglement between a single qubit and the rest can be calculated from the mean of the collective spin operators. This allows the possibility of efficiently measuring entanglement dynamics in an experimental setting. We consider a deeply quantum regime and show that signatures of chaos are present in the dynamical entanglement for parameters accessible in an experiment that we propose using cold atoms. The evolution of the entanglement depends on the support of the initial state on regular versus chaotic Floquet eigenstates, whose phase-space distributions are concentrated on the corresponding regular or chaotic eigenstructures. We include the effect of decoherence via a realistic model and show that the signatures of chaos in the entanglement dynamics persist in the presence of decoherence. In addition, the classical chaos affects the decoherence rate itself.

DOI: 10.1103/PhysRevA.78.042318 PACS number(s): 03.67.Bg, 05.45.Mt, 42.50.Ct, 03.65.Yz

I. INTRODUCTION

In classical mechanics, the chaotic behavior predicted for nonintegrable systems can be qualitatively different from the regular dynamics of integrable systems [1]. The concept of regular versus chaotic dynamics at the quantum level has been more difficult to define as there is no clear measure of chaos in the quantum regime. Understanding the correspondence between quantum and classical evolutions in chaotic systems is a central problem in quantum mechanics and a major focus of the field of quantum chaos. From a practical perspective, recent work [2] has shown that classical chaos can affect the implementation of quantum computing algorithms, and has fueled interest in identifying the effects of chaos on quantum information theoretic properties such as quantum correlations or entanglement, and fidelity [3]. Entanglement is thought to be a fundamental resource for many quantum information processing applications, and the effect of chaos on the dynamical generation of entanglement has been a topic of several studies [4–13]. The presence of chaos can also increase the rate of entanglement generation between a system and its environment [14,15], leading to increased decoherence and possibly stricter limitations on coherent quantum information processing.

In this paper, we explore the effect of chaos on entanglement and decoherence in a quantum kicked top [16,17]. We treat the kicked top as a collection of spin-1/2 systems or qubits and find an efficient measure of entanglement between a single qubit and the rest. We focus on dynamics in a deeply quantum regime rather than the more commonly studied semiclassical regime, in order to probe the boundary between quantum and classical behavior and try and identify truly "quantum" chaos. Our motivation to study the quantum regime also arises from the possibility of performing experimental studies of this system. We identify signatures of chaos in the entanglement dynamics in a quantum regime that can be accessed in an experiment that we propose using cold atoms.

The quantum kicked top has become a standard paradigm for theoretical studies of quantum chaos but has not yet been studied in experiments. Here, we propose and analyze a possible experimental realization based on cesium atomic spins interacting with laser light and a pulsed magnetic field. The kicked top Hamiltonian can be implemented by controlling the evolution of the ground hyperfine (electron+nuclear) spin of each cesium atom via laser and magnetic field interactions. With a maximum ground state hyperfine spin of $F=4$ [18], this system lies far from the semiclassical regime that is usually considered, since the size of $\hbar$ relative to the total phase space is roughly 0.1. We study entanglement dynamics for parameters accessible with this system. Our analysis shows that signatures of chaos can be observed even if the atoms undergo decoherence due to spontaneous emission, and that chaos affects the decoherence rate itself. The cold atom experimental system provides a clean setting in which to perform fundamental studies of quantum-classical correspondence and develop a toolbox of quantum control of multiqubit systems undergoing complex dynamics.

A quantum kicked top with total angular momentum j can be decomposed into $N=2j$ spin-1/2 subsystems (qubits) [9]. We focus on the entanglement between a single qubit and the remaining $k=N-1$ qubits (henceforth called $1:k$ entanglement). The $1:k$ entanglement is of relevance to our proposed experiment with cold atoms because, as we will show, it corresponds to entanglement between electron and nuclear spin in a single atom. Measurement of entanglement is usually experimentally challenging as it would require performing complete state tomography. For the case of the kicked top, we derive a simple expression for a $1:k$ entanglement measure in terms of the expectation values of the total spin of the N qubits. Hence, the $1:k$ entanglement can be efficiently monitored by simply measuring the evolution of the mean total spin vector, thereby avoiding the need to perform

complete state tomography. Although this result is generally applicable to any kicked top experimental realization, it is particularly useful for the cold atom experiments proposed here, in which the evolution of the mean spin vector can be efficiently measured in real time [19,20].

We have performed numerical simulations of the kicked top dynamics to study the evolution of entanglement. In order to compare quantum and classical dynamics, we pick initial quantum states that are localized in regular versus chaotic regions of the classical phase space and analyze the evolution of the $1:k$ entanglement as we vary the initial conditions from the regular to the chaotic regime. Our results show that the long term $1:k$ entanglement dynamics exhibit signatures of classical chaos even in the extreme quantum regime considered here. Initial states localized in regular regions of the classical phase space exhibit quasiperiodic collapses and revivals, whereas initial localized states centered in chaotic regions quickly spread out and do not exhibit quasiperiodic entanglement dynamics. These signatures are similar to those previously identified in the $2:k$ entanglement [9] between two qubits and the rest in a semiclassical regime. We explain the entanglement behavior by extending the analysis in [10] to the quantum regime. Quasiperiodicity versus irrregular dynamics depends on the support of the initial state on regular versus chaotic eigenstates of the Floquet evolution operator as shown in [10]. The differences in eigenstate decomposition for initial states centered in regular versus chaotic regions are limited by the small size of the spin considered here, and has no significant effect on the initial rate of entanglement generation as is the case for the semiclasscial regime [10]. Nevertheless we find surprisingly clear signatures of regular versus chaotic dynamics in the long-term evolutions. Regular and chaotic structures of the mixed classical phase space are also clearly evident in the Husimi phase-space distributions [21] of the Floquet eigenstates in the quantum regime.

In addition to unitary evolution, we also consider the more realistic case of nonunitary dynamics when the kicked top system is coupled to its environment. Our simulations of the entanglement dynamics include the effect of decoherence through a master equation description that accurately simulates photon scattering in our cold atom system. Analysis of the negativity, a measure of entanglement for mixed states, shows that, although decoherence due to coupling with the environment acts to reduce the overall $1:k$ entanglement, striking differences in the entanglement dynamics in regular versus chaotic regimes can persist for times longer than the decoherence time. Furthermore, the rate of decoherence itself is slower in a regular regime than in a chaotic regime. Effects of chaos on the decoherence rate were previously studied in [14,15,22–24] using general models of decoherence in a semiclassical regime. Here we use a *realistic* and accurate model to verify qualitatively that classical chaos indeed affects the decoherence rate in a physical system, even in a deeply quantum regime. Our proposed cold atom implementation would be the first to allow studies of decoherence and entanglement dynamics in a chaotic system.

The paper is organized as follows: In Sec. II we describe the basic features of the standard quantum kicked top and the corresponding classical system, which can exhibit chaos for certain dynamical parameters. Section III discusses the efficient measurement of $1:k$ entanglement dynamics and the possibility of experimental studies of entanglement with cold atoms. In Sec. IV we present an analysis of signatures of chaos in the entanglement dynamics of the kicked top for a regime accessible in the cold atom system. We build on our previous analysis of the kicked top [10] and identify regular and chaotic eigenstates whose distributions are concentrated on the classical phase-space structures in Sec. V. The relationship between decoherence, entanglement, and chaos is analyzed in Sec. VI. We present a summary and our conclusions in Sec. VII.

II. QUANTUM KICKED TOP AND ITS CLASSICAL LIMIT

The Hamiltonian for a quantum kicked top is given by [16,17]

$$H = \frac{\kappa}{2j\tau}J_x^2 + pJ_y\sum_{n=-\infty}^{\infty}\delta(t-n\tau). \tag{1}$$

Here, the operators J_x, J_y, and J_z are angular momentum operators obeying the commutation relation $[J_i,J_j]=i\hbar\epsilon_{ijk}J_k$. The Hamiltonian describes a series of kicks given by the linear J_y term interspersed with torsions due to the nonlinear J_x^2 term. The time between kicks is τ, the angle of turn per kick is given by p, and the strength of the twist is determined by κ. The magnitude $J^2=j(j+1)\hbar^2$ is a constant of the motion.

The classical map from kick to kick can be obtained from the Heisenberg evolution equations for the expectation values of the angular momentum operators,

$$\langle J_i\rangle_{n+1} = \langle U^\dagger J_i U\rangle_n. \tag{2}$$

U is the Floquet operator describing unitary evolution from kick to kick,

$$U = \exp(-i\kappa J_x^2/2j)\exp(-ipJ_y), \tag{3}$$

where the energy is henceforth rescaled such that $\tau=1$. The equations describing the evolution of the mean J_x, J_y, and J_z involve functions of second moments of the angular momentum operators, whose evolution in turn depends on third moments in an infinite hierarchy of equations. In order to obtain the classical mapping, we factorize all second and higher moments into products of the mean values (first moments) of the angular momentum operators. This corresponds to localization of the state to a point in the classical limit and breaks the infinite hierarchy of equations at the level of first moments. Then, by defining the normalized variables $X=\langle J_x\rangle/j$, $Y=\langle J_y\rangle/j$, and $Z=\langle J_z\rangle/j$, we can write down the classical mapping

$$X_{n+1} = X_n\cos(p) + Z_n\sin(p),$$

$$Y_{n+1} = Y_n\cos(\kappa\tilde{X}_n) - \tilde{Z}_n\sin(\kappa\tilde{X}_n),$$

$$Z_{n+1} = \tilde{Z}_n\cos(\kappa\tilde{X}_n) + Y_n\sin(\kappa\tilde{X}_n),$$

$$\tilde{Z}_n = Z_n\cos(p) - X_n\sin(p),$$

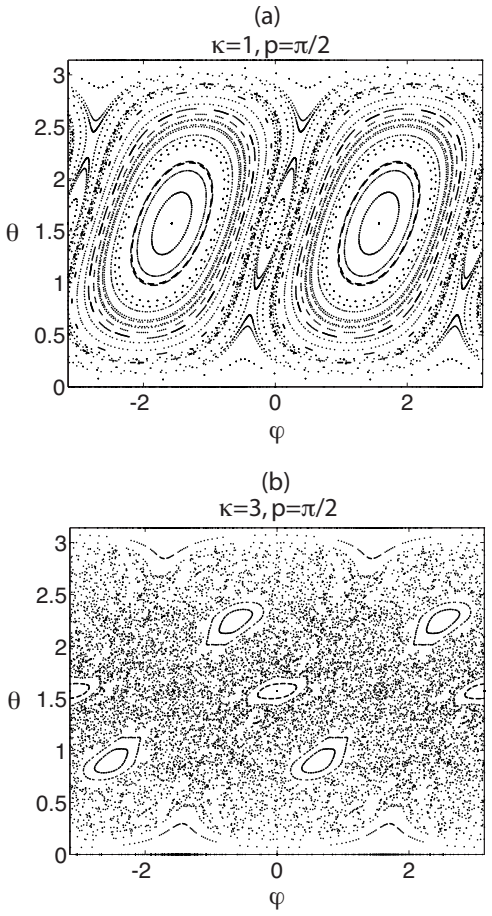

FIG. 1. Stroboscopic phase-space maps of the classical kicked top at different values of κ for kick strength $p=\pi/2$. The spherical coordinates (θ,ϕ) are plotted (units of radians) after each kick for 144 initial conditions, each evolved for 150 kicks. (a) For smaller κ, the phase space is dominated by regular orbits. (b) At larger κ, regular orbits are embedded in a sea of chaotic trajectories.

$$\tilde{X}_n = X_n \cos(p) + Z_n \sin(p). \tag{4}$$

$\tilde{X}_n$ and $\tilde{Z}_n$ are the angular momentum variables subsequent to the kick but before the action of the twist.

The parameter κ is the chaoticity parameter in the classical kicked top. For $p=\pi/2$, Fig. 1 shows how κ affects the kick-to-kick stroboscopic dynamics of the classical variables $\theta=\cos^{-1} Z$, $\phi=\tan^{-1}(Y/X)$. When $\kappa=1$, the stroboscopic phase space is dominated by islands of regular (periodic) motion [Fig. 1(a)]. As κ is increased, the phase space becomes mixed with regular islands embedded in a sea of chaotic trajectories [Fig 1(b)]. For even larger values of κ, the system eventually becomes globally chaotic.

III. MEASUREMENT OF ENTANGLEMENT IN THE KICKED TOP

A. 1:k entanglement measure

We now focus on the dynamical evolution of entanglement in the quantum kicked top. The total spin j can be considered as a system of $N=2j$ qubits with

$$J_\alpha = \sum_{i=1}^{N} \frac{\sigma_{\alpha_i}}{2}, \quad \alpha = x,y,z, \tag{5}$$

where σ_{α_i} are the Pauli operators for the ith qubit. For initial states that are symmetric under permutations of the identical qubits, the kicked top operator acts collectively on all N qubits, preserving the symmetry of the N-qubit state. This allows us to write the spin expectation values for any single qubit as

$$\langle s_\alpha \rangle = \frac{\langle \sigma_\alpha \rangle}{2} = \frac{\langle J_\alpha \rangle}{2j}. \tag{6}$$

For an overall pure state, the entropy of the reduced state $\tilde{\rho}$, of a single qubit is a measure of $1:k$ entanglement between a single qubit and the remaining $k=N-1$ qubits. For convenience we study the linear entropy, $S=1-\mathrm{Tr}[\tilde{\rho}^2]$. S ranges from 0 for separable states to $1/2$ for maximally entangled states. Since $\tilde{\rho}$ is a 2×2 density operator, it can in general be expressed in terms of the Pauli matrices and the identity matrix as [18]

$$\tilde{\rho} = \frac{1}{2} + \langle \mathbf{s} \rangle \cdot \boldsymbol{\sigma}, \tag{7}$$

where $\langle \mathbf{s} \rangle$ is the mean spin vector of the qubit. Substituting the expression for $\langle \mathbf{s} \rangle$ from Eq. (6) into Eq. (7), $\tilde{\rho}$ can be expressed in terms of the collective angular momentum operators as

$$\tilde{\rho} = \frac{1}{2} + \frac{1}{2j} \langle \mathbf{J} \rangle \cdot \boldsymbol{\sigma}. \tag{8}$$

The linear entropy $S=1-\mathrm{Tr}[\tilde{\rho}^2]$ is then easily computed to be

$$S = \frac{1}{2}\left[1 - \frac{1}{j^2}(\langle J_x \rangle^2 + \langle J_y \rangle^2 + \langle J_z \rangle^2) \right]. \tag{9}$$

Measurement of the expectation values of the angular momenta, $\langle J_\alpha \rangle$, thus provides us with enough information to calculate S, which is a measure of the $1:k$ entanglement, without having to perform complete state tomography to reconstruct the entire multiqubit density operator. We also note that the function S is identical to the generalized entanglement with respect to the angular momentum observables—an entanglement measure that is independent of subsystem division [25]. Furthermore, the linear entropy function is directly related to the "extent" or average spread of the state on the sphere. For a state that is highly localized on the sphere, the sum of the mean values of the angular momentum operators with be close to j so the entropy S will be close to 0. On the other hand, for a highly delocalized state, the mean values of the angular momentum operators in Eq. (9) approaches 0 and the value of S approaches its maximum of $1/2$.

B. Experiments with cold atoms

An attractive physical system in which to realize a quantum kicked top is the total hyperfine (electron+nuclear) spin

[18] of the electronic ground state of an individual atom. In particular, we propose using samples of laser cooled alkali-metal atoms to perform experiments on ensembles of identical kicked tops. The atomic spins can be initialized by optical pumping, and manipulated in a controlled manner by Larmor precession in applied magnetic fields, and electric dipole interaction with an applied laser field. Furthermore, one can perform polarization spectroscopy on the driving field to probe the spins in real time without perturbing the dynamics [19]. These tools have already been used to demonstrate nonlinear spin dynamics [20], quantum state reconstruction [26], and quantum state control [27] with cesium atomic spins. In the following, we briefly describe how to realize the kicked top with this system.

In the low saturation, large detuning limit, the electric dipole interaction between a single atom and a monochromatic laser field is described by a light shift

$$U = -\frac{1}{4}\mathbf{E}^* \cdot \hat{\boldsymbol{\alpha}} \cdot \mathbf{E}, \tag{10}$$

where $\mathbf{E}=\mathrm{Re}(\mathbf{E}e^{-i\omega t})$ is the electric field, and where the atomic polarizability $\hat{\boldsymbol{\alpha}}$ is a rank-two tensor operator that can be decomposed into irreducible components of rank 0, 1, and 2 [28,29]. Here, we consider alkali-metal atoms restricted to a hyperfine ground state of given angular momentum F, where $\mathbf{F}=\mathbf{I}+\mathbf{S}$ and $\mathbf{F}^2=F(F+1)\hbar^2$ [18]. Here $\mathbf{I}$ is the nuclear spin and $\mathbf{S}$ is the electron spin. Specifically, for cesium which has a nuclear spin of $I=7/2$ and electron spin of $s=1/2$, F can be either 4 or 3. Here we focus on the $F=4$ ground state hyperfine manifold. The light shift U is then an operator acting in a $(2F+1)$-dimensional manifold, separable into three contributions from the irreducible components of $\hat{\boldsymbol{\alpha}}$ [28,29].

The rank-0 contribution is a scalar interaction which does not couple to the spin degrees of freedom and therefore can be ignored. The rank-1 contribution is an effective Zeeman interaction of the form $\mathbf{B}_{\mathrm{eff}}\cdot\mathbf{F}$, where $\mathbf{B}_{\mathrm{eff}}$ is proportional to the ellipticity of the laser field polarization [28]. For a linearly polarized driving field, this term disappears, leaving only the rank-2 contribution. Choosing linear polarization in the x-direction, the overall light shift is then quadratic in a component of the hyperfine spin as required for the kicked top [26,27,29],

$$U = \frac{\beta\gamma_s}{\hbar}F_x^2. \tag{11}$$

Here, γ_s is the single-atom photon scattering rate, which depends on the laser intensity I, detuning Δ, transition linewidth Γ, and saturation intensity I_0 [30] as $\gamma_s=(\Gamma^3/8\Delta^2)(I/I_0)$ [28,29]. The parameter β is a measure of the relative time scales for unitary evolution and decoherence, and depends on the atomic species and the frequency of the driving field. It takes on a maximum value of 8.2 for cesium atoms driven at a frequency in between the two hyperfine components of the $D1$ line at 894 nm [26]. Comparing Eqs. (1) and (11), we see that the strength of the chaoticity parameter is related to the system parameters by

$$\kappa = \frac{2\beta\gamma_s}{\hbar}F\tau. \tag{12}$$

Thus larger values of κ are accompanied by higher rates of decoherence through photon scattering, and this limits the time over which one can observe unitary evolution of the system.

The kicking term in the Hamiltonian of Eq. (1) can be implemented by a train of magnetic field pulses separated by a time τ. This results in a Zeeman interaction of the form $g\mu_B\mathbf{B}\cdot\mathbf{F}\Sigma_n\delta(t-n\tau)$, where g is the g factor, μ_B is the Bohr magneton, and B is the strength of the magnetic field. The finite bandwidth limitations of magnetic coils and drivers prevent the application of true δ kicks, but it is not difficult in practice to keep the kick duration T much shorter than the time τ between kicks so that the δ-kick approximation remains valid. The angle of the turn per kick depends on the Larmor frequency Ω_L of the applied magnetic field,

$$p = \Omega_L T. \tag{13}$$

Hence, by adjusting the laser intensity, detuning, Larmor frequency, kick spacing, and duration, one can explore a whole range of kicked top parameters κ and p.

To observe quantum dynamics in different regions of the classical phase space, we start with initial spin coherent states [31], which are rotations of the state $|j,m=j\rangle$ having maximum projection along the z axis,

$$|\theta,\phi\rangle = e^{i\theta[J_x\sin\phi - J_y\cos\phi]}|j,m=j\rangle. \tag{14}$$

The expectation value of the spin in this state is given by $\langle\mathbf{J}\rangle=(j\sin\theta\cos\phi, j\sin\theta\sin\phi, j\cos\theta)$. In the qubit description, these states are separable with zero entanglement between qubits. In our atomic system, the total angular momentum $\mathbf{F}$ is the sum of a large nuclear spin ($I=7/2$ for cesium) and a valence electron spin-1/2 system (qubit) whose reduced state can be described as in Eq. (7). Starting with initial spin coherent states and restricting ourselves to the manifold of maximum F ($F=4$ for cesium), the quantity S in Eq. (9) is then a measure of the entanglement between electron and nuclear spin, which can be experimentally measured by monitoring the mean collective angular momentum $\langle\mathbf{F}\rangle$ through, e.g., Faraday spectroscopy [19]. Alternatively one can perform complete quantum state reconstruction of the overall electron+nuclear spin state [26]. This opens up the possibility of computing other entanglement measures such as negativity, and of monitoring decoherence by calculating the overall state purity.

IV. DYNAMICAL ENTANGLEMENT AND CHAOS

We analyze here the $1:k$ entanglement dynamics of the kicked top described by the Hamiltonian in Eq. (1). We pick the magnitude of the angular momentum j to be 4 to correspond to the $F=4$ hyperfine manifold in the cesium ground state. This puts the system far from the semiclassical regime of large j ($j>100$) that has been studied in previous work on signatures of chaos [9,10]. Even in this deeply quantum regime with $j=4$, we can clearly identify the effect of chaos in the entanglement dynamics.

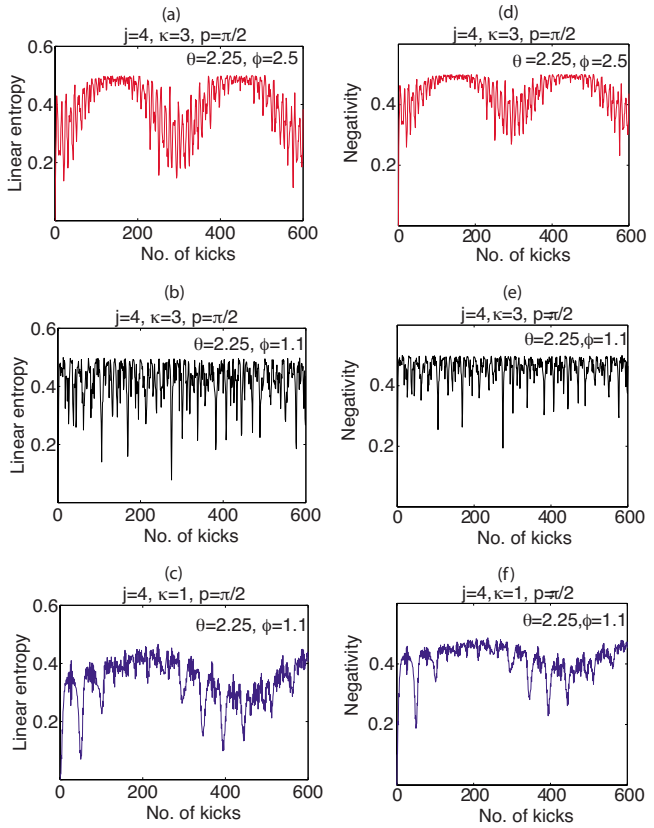

FIG. 2. (Color online) Evolution of the linear entropy S [(a)–(c)] and the negativity N [(d)–(f)], for initial spin coherent states $|\theta,\phi\rangle$ centered in regular versus chaotic regimes of the classical phase space. θ,ϕ are in units of radians. See the text for details.

For $\kappa=3$, $p=\pi/2$, we pick an initial spin coherent state centered on a regular island of Fig. 1(b) with $\theta=2.25$, $\phi=2.5$. The resulting evolution of the entanglement measure S shows quasiperiodic behavior [Fig. 2(a)] with collapses and revivals in the entanglement. In contrast, for an initial state centered in the chaotic sea of Fig. 1(b) with $\theta=2.25$, $\phi=1.1$, the quasiperiodic behavior disappears [Fig. 2(b)] and the evolution is irregular. For this same initial state with $\theta=2.25$, $\phi=1.1$, if we change κ to 1, the classical dynamics becomes regular again [Fig. 1(a)], and correspondingly, quasiperiodic motion is recovered in the entanglement dynamics in Fig. 2(c). For both the regular and chaotic dynamics, entanglement at first increases as the initially localized state starts spreading over the phase space. However, for the states initialized in regular regimes, the dynamics causes the state to relocalize periodically, causing a reduction in entanglement. This periodicity is more clearly illustrated in the Fourier transform of the entanglement dynamics as shown in Fig. 3. The frequency spectrum for initial states in a regular regime have a few peaks whereas the spectrum for the initial state in the chaotic regime is spread over a wide range of incommensurate frequencies. In the regular regime the frequency spectrum also has peaks close to zero frequency, which leads to long term periodic evolution. Although Fig. 3(c) shows more peaks than Fig. 3(a), the peaks are quite evenly spaced leading to more periodic, regular evolution and less dephasing. We explore this periodicity in more detail in the following section.

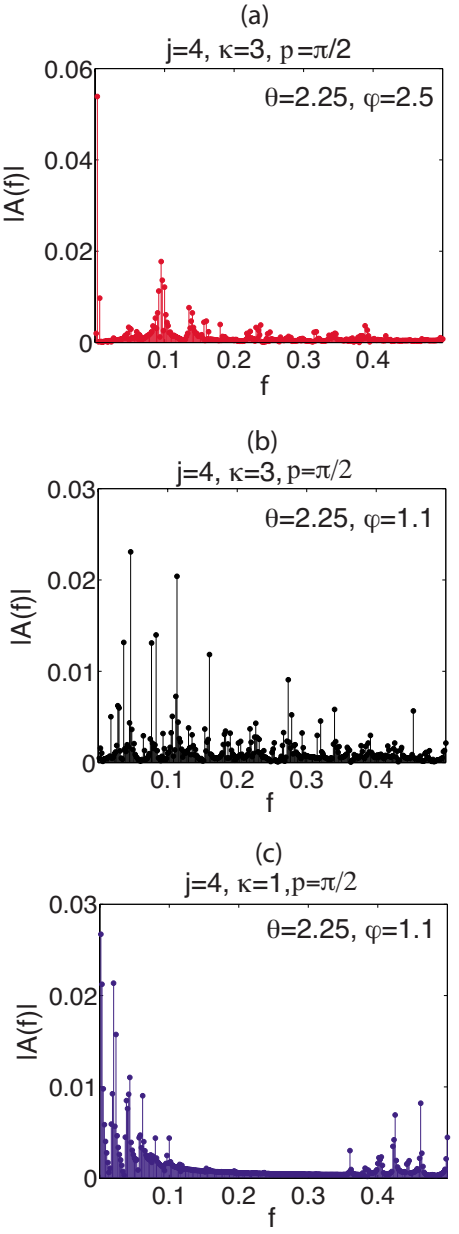

FIG. 3. (Color online) Absolute value of the Fourier transform of the linear entropy S, in Figs. 2(a)–2(c). The frequency f is in units of 1/(kicks). See the text for further details.

We also compute a different measure of entanglement—namely, the negativity defined as [32]

$$N = \frac{\|\rho_T\| - 1}{2}, \tag{15}$$

where ρ_T is the partial transpose of the overall state, $\rho_{T_{m\mu n\nu}} = \rho_{n\mu m\nu}$. Here ρ is expressed in a product basis $|m\rangle \otimes |\mu\rangle$, where $|m\rangle$ is a basis for the single qubit (electron spin) subsystem and $|\mu\rangle$ is a basis for the remaining qubits (nuclear spin). The trace norm is defined to be

$$\|\rho_T\| = \mathrm{Tr}[\sqrt{\rho_T^\dagger \rho_T}]. \tag{16}$$

Negativity is an entanglement monotone and has been shown to be a valid entanglement measure [33]. One problem with

negativity is that it cannot distinguish between separable (unentangled) states and bound or PPT entangled states [34] that have a positive partial transpose [35] since in both cases the negativity is zero. However in our case, the kicked top Hamiltonian does not generate such PPT entangled states, so we can use negativity as an unambiguous entanglement measure to compare to the linear entropy. Whereas entropy is a measure of entanglement only for pure states, negativity can be used as an entanglement measure for mixed states. We can thus use this measure later in Sec. V to understand the entanglement dynamics when we include photon scattering in our model and the initial pure state becomes mixed due to decoherence. The evolution of the negativity for the three initial states considered in Figs. 2(a)–2(c) is shown in Figs. 2(d)–2(f). The qualitative behavior exactly matches the evolution of the linear entropy. We can identify collapses and revivals in the dynamics for initial states in a regular regime and irregular evolution for states initially in the chaotic sea. The Fourier transform of the negativity is similar to that shown in Fig. 3, so it is not explicitly shown again.

The three initial states analyzed above are representative of the general behavior of entanglement in regular versus chaotic regions. The entanglement dynamics changes more or less smoothly from regular quasiperiodic evolution to irregular evolution as we scan through initial spin coherent states from regular to chaotic regions. To illustrate this, Fig. 4(a) shows the average entanglement over 600 kicks as a function of initial conditions (θ,ϕ) scanned along the line $\theta=2.25$. The quasiperiodic behavior for initial states in the regular islands leads to lower average entanglement as compared to initial states in the chaotic sea. The initial transient dynamics does not significantly affect the average value. In Fig. 4(a), the regular islands can be clearly identified by the dips in the average entanglement. Conversely, in order to confirm that the entanglement behavior is connected to the level of chaoticity of the classical map, we scan through the chaoticity parameter κ for a fixed initial condition $\theta=2.25$, $\phi=1.1$. The time average entanglement as a function of κ is shown in Fig. 4(b). As the chaoticity parameter is increased, the average entanglement increases. The dips in average entanglement reflect the occasional appearance of periodic orbits as fixed points in the classical phase-space bifurcate in the approach to global chaos.

To further confirm the correlation between the time averaged entanglement and classical chaos, we plot the largest classical Lyapunov exponent [36,37] in Fig. 5 as a function of initial conditions [Fig. 5(a)] and κ [Fig. 5(b)]. The Lyapunov exponent characterizes the level of classical chaos by quantifying the rate of exponential divergence of initially neighboring trajectories in the classical phase space. It is zero in regular regimes and increases with the degree of chaoticity of the system. A comparison of Fig. 4 to Fig. 5 shows the clear correlation between the average entanglement and the Lyapunov exponent even though we are far from the semiclassical regime. The dips in Figs. 4(a) and 4(b) correspond to the dips in Figs. 5(a) and 5(b). The average entanglement increases with κ like the Lyapunov exponent but the maximum entanglement is limited to 0.5. There are also some other differences. The Lyapunov exponent is zero for initial conditions starting in the regular islands or

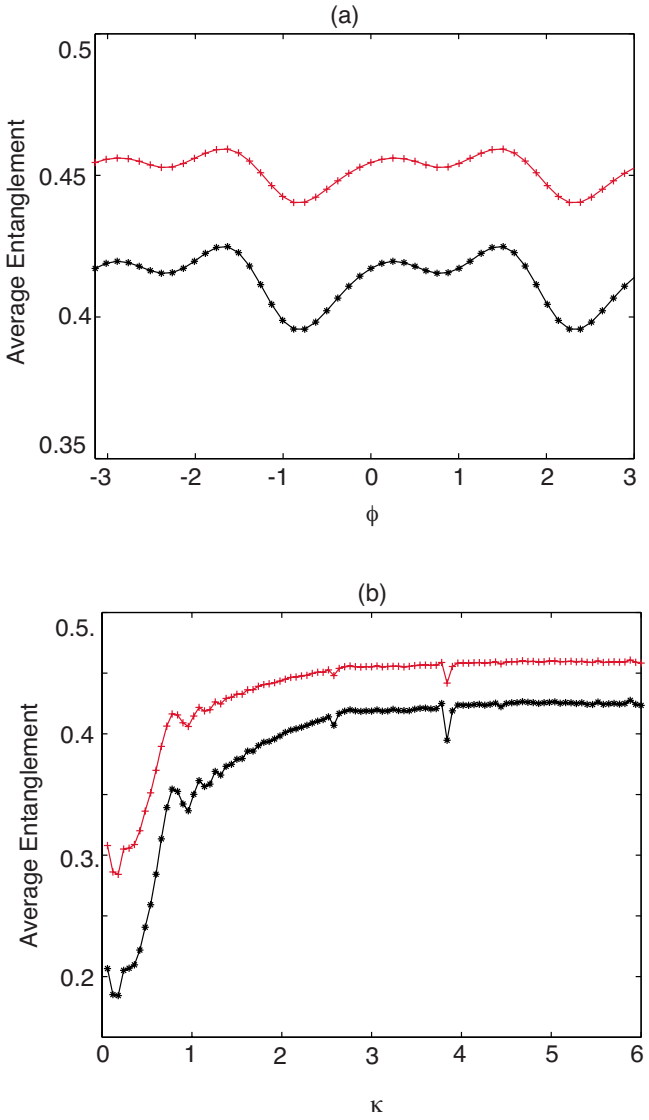

FIG. 4. (Color online) Time averaged entanglement measured by both entropy (stars) and negativity (pluses) reflects regular and chaotic classical structures as (a) the location of the initial spin coherent state is varied along the line $\theta=2.25$, $-\pi<\phi<\pi$ for constant $\kappa=3$, $p=\pi/2$ and (b) κ is varied keeping the initial state constant at $|\theta=2.25,\phi=1.1\rangle$. The average is taken over 600 kicks. θ,ϕ are in units of radians. For further details, see the text.

when κ is smaller than 2.4. The initial quantum on the other hand, is not a point in phase space, but has some spread in phase space. The corresponding average entanglement is smaller but not zero in regular regions but varies more smoothly because of the spread of the state in phase space. If the value of j is increased so that we move into a more semiclassical regime, the correspondence becomes better and the dips in entanglement in the regular islands become deeper and closer to zero. This behavior is examined more closely in the next section.

V. ANALYSIS OF FLOQUET EIGENSTATES

In previous work [9], we had identified similar signatures of chaos in the $2:k$ entanglement dynamics of two qubits

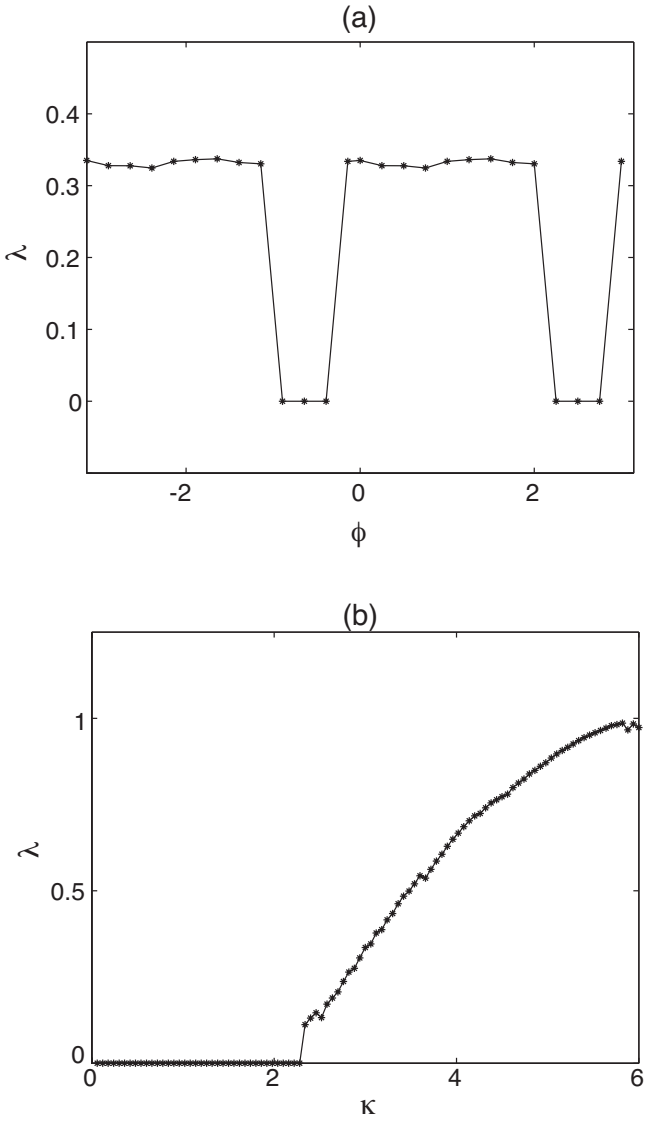

FIG. 5. Largest classical Lyapunov exponent, λ as (a) the initial condition is varied along the line $\theta=2.25$, $-\pi<\phi<\pi$ for constant $\kappa=3$, $p=\pi/2$ and (b) κ is varied keeping the initial condition constant at $\theta=2.25$, $\phi=1.1$. θ,ϕ are in units of radians.

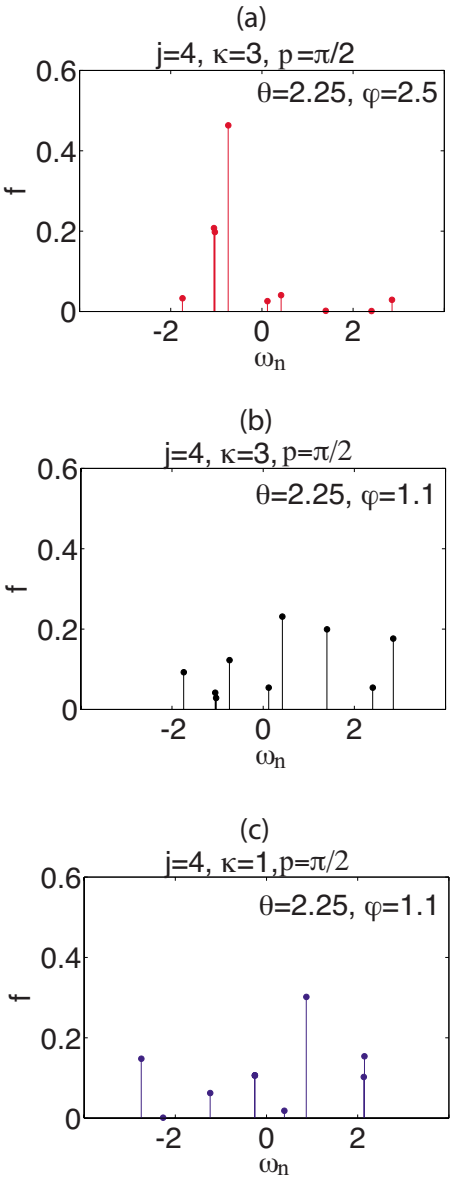

FIG. 6. (Color online) Overlap $f=|\langle u_n|\theta,\phi\rangle|^2$ of each of the three initial spin coherent states $|\theta,\phi\rangle$ in Fig. 2 with Floquet eigenstates $|u_n\rangle$ corresponding to eigenfrequencies ω_n. Initial states in a regular region (a),(c) have support on a few regularly spaced or degenerate eigenstates, while the state in the chaotic sea (b), has support on a larger number of chaotic eigenstates with irregularly spaced eigenfrequencies. θ,ϕ are in units of radians.

with the remaining qubits for a collection of $N>50$ qubits. Here, we have shown that these features are generic and can also be observed in the $1:k$ entanglement between a single qubit and the rest. Furthermore, these signatures are surprisingly persistent even for the case $j=4$ corresponding to only eight qubits, which is far from the semiclassical regime. Reference [10] explained these universal signatures of chaos by showing that in a semiclassical regime, the eigenstates $|u_n\rangle$, of the kick-to-kick Floquet evolution operator [Eq. (3)] can be classified as "regular" or "chaotic." An initial state centered in a regular island has support on a few almost degenerate regular eigenstates that give rise to quasiperiodic motion involving a few regularly spaced eigenfrequencies, whereas a state initially localized in a chaotic sea can be decomposed into a number of chaotic eigenstates with a broad spectrum of incommensurate frequencies contributing to the dynamics.

Here, we test the above argument in the quantum regime. Figure 6 shows the eigenstate decomposition $f=|\langle u_n|\theta,\phi\rangle|^2$ of the three initial states whose dynamics are shown in Fig. 2. Each eigenstate is labeled by the corresponding eigenphase ω_n,

$$U|u_n\rangle = e^{i\omega_n}|u_n\rangle, \tag{17}$$

where U is the Floquet evolution operator [Eq. (3)]. The regular initial state of Figs. 2(a) and 2(d) has support on a few regular almost degenerate eigenstates [Fig. 6(a)], while the chaotic initial state of Figs. 2(b) and 2(e) has support on eigenstates with a broader spectrum of irregularly spaced fre-

quencies [Fig. 6(b)]. For the regular motion, the finite number of frequencies present in the frequency spectrum of $S(t)$ can be identified as sums of differences between eigenfrequencies of the regular eigenstates on which the initial state has support [10]. In the chaotic case, the large number of distinct eigenfrequency-difference sums give rise to a broader power spectrum. The regular state in Fig. 6(c) also shows support mostly on a single eigenstate and some support on almost degenerate eigenstate pairs. Although the spectrum looks similar to the chaotic state of Fig. 6(b), the larger number and irregular spread of eigenfrequencies in the chaotic state is sufficient to make the evolution much more irregular than the regular case. Upon closer examination, we find that unlike the chaotic case, the eigenfrequency spacing of the dominant states in Fig. 6(c) is quite regular. This regular spacing and the larger support on a single eigenstate leads to regular entanglement dynamics, with periodic revivals or "rephasing" of the evolutions of the different component eigenfrequencies, as seen in Fig. 2. Furthermore, support on the almost degenerate eigenstate pairs lead to long term periodic behavior, which is missing in the chaotic case. The irregular oscillations on a fast time scale are due to the small but nonzero support on the remaining eigenstates.

Due to the small value of j of 4, there are only a small total number of regular and chaotic eigenstates, so the chaotic power spectrum will not be completely flat and the dynamics will show some quasiperiodic behavior. Furthermore, due to the mixed nature of the phase space, some eigenstates have overlap on regular as well as chaotic regions and can partially contribute to initial states in both regular and chaotic regions. Thus the differences between regular and chaotic regimes are not as clearly delineated in this deeply quantum regime, compared to a semiclassical regime. Nevertheless, the regular and chaotic regions of the classical phase space can be identified by the support of the initial state on the Floquet eigenstates. To verify this, in Fig. 7 we plot the quantity

$$s = \sum_n |\langle u_n|\theta,\phi\rangle| \tag{18}$$

as a function of initial conditions (θ,ϕ) along the line $\theta=2.25$, for $\kappa=3$, $p=\pi/2$. This quantity measures the number of eigenstates on which the initial state has support. s is close to the maximum value of 3 in chaotic regions where the initial state is a superposition of a large number of eigenstates. s is a minimum of 1 if the initial state is supported only on a single eigenstate. Therefore, when the initial state is in a regular regime with support on only a few eigenstates, s is closer to its minimum value. Thus s gives us a quantitative measure which identifies chaotic versus regular dynamics. As can be seen in Fig. 7, the dips in s correspond to the regular regions in the mixed classical phase space and correlate perfectly with the time averaged entanglement, as well as the classical Lyapunov exponent in Fig. 5(a).

To further confirm the correspondence between the classical phase space and the quantum eigenstates, Fig. 8 shows the Husimi quasiprobability distribution of the eigenstates with largest overlap with each of the three initial states considered in Fig. 2. The Husimi distributions show an overlap of a state $|u_n\rangle$ with spin coherent states [21],

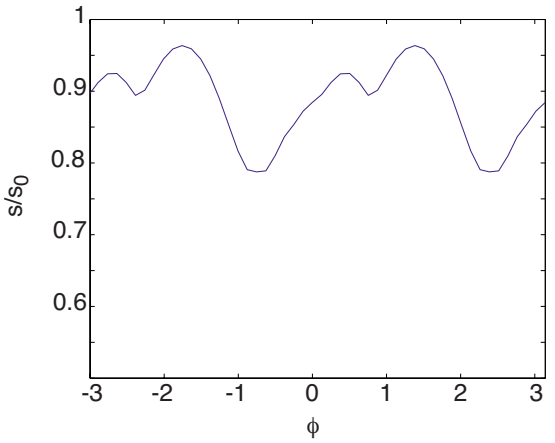

FIG. 7. (Color online) Support on the Floquet eigenstates, $|u_n\rangle$, $s=\Sigma_n|\langle u_n|\theta,\phi\rangle|$. The initial spin coherent state $|\theta,\phi\rangle$ is varied along the line $\theta=2.25$, $-\pi<\phi<\pi$ with fixed $\kappa=3$, $p=\pi/2$. s is normalized with respect to its maximum value of $s_0=3$, corresponding to the case of equal support over all eigenstates. s/s_0 has a minimum of $1/3$ when the state has support on a single eigenstate. The dips correspond therefore to the location of the regular islands in the classical phase space of Fig. 1, as the initial state has support only on a few regular eigenstates. θ,ϕ are in units of radians.

$$P(\theta,\phi) = \frac{2j+1}{4\pi}|\langle\theta,\phi|u_n\rangle|^2. \tag{19}$$

The distributions clearly show that the probability is concentrated on the classical phase-space structures shown in Fig. 1. For regular eigenstates they are concentrated along periodic orbits whereas for chaotic eigenstates they are delocalized in the chaotic sea. Thus, although quantum chaos typically deals with semiclassical techniques to explore quantum-classical correspondence, our theoretical analysis provides evidence that very clear signatures of classical chaos can be present in regimes far from the classical or even semiclassical regimes.

A second signature of classical chaos predicted by the semiclassical analysis is that the initial increase in entanglement is faster for the state starting in the chaotic sea than for those starting in regular regions [10]. In the chaotic regime the initial rate of increase was predicted to be exponential due to the contribution of a large number of incommensurate eigenfrequencies to the dynamics. In the quantum system considered here, due to the small size of the Hilbert space, there are not enough eigenfrequencies to give rise to an initial exponential increase in entanglement. Furthermore, the initial spin coherent states are not well localized in the phase space and therefore tend to have support on both regular and chaotic regions. This in turn tends to wash out differences in the initial rate of entanglement generation. In fact, we find no significant difference in the initial increase in entanglement for states in regular versus chaotic regions. Our studies thus not only serve to identify the correspondence between quantum and classical descriptions, but also highlight the differences inherent in quantum and classical systems.

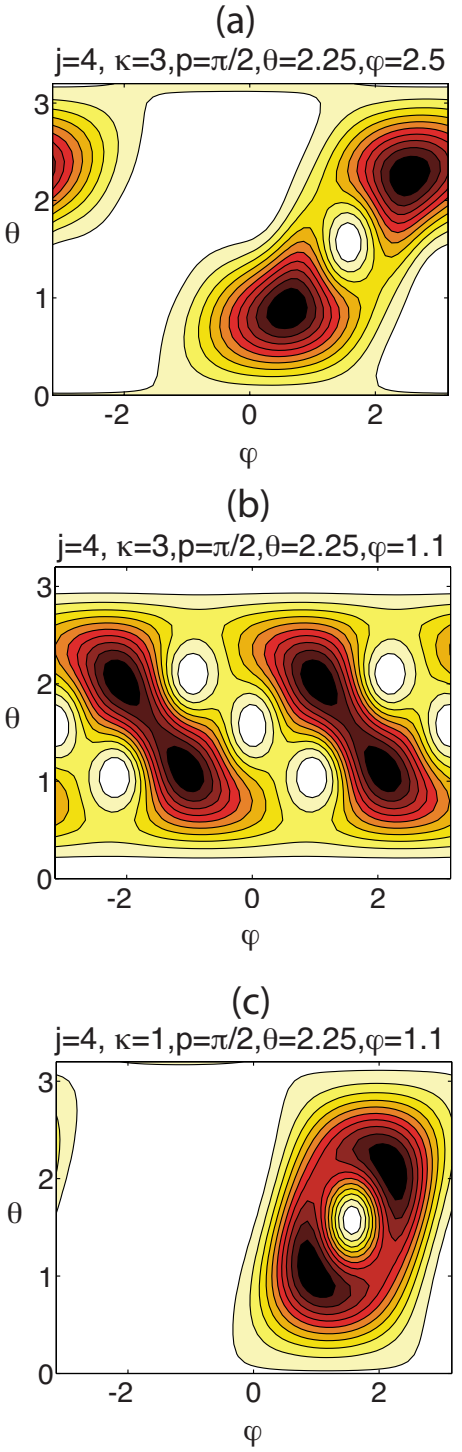

FIG. 8. (Color online) Husimi distribution of the Floquet eigenstate having the largest overlap with each of the three initial states (a)–(c) considered in Fig. 2. Solid lines are contours of equiprobability distribution, and darker regions indicate larger probability. A comparison with Fig. 1 clearly shows concentration of the distributions along the classical phase-space structures. θ, ϕ are plotted in units of radians.

VI. DYNAMICAL ENTANGLEMENT AND DECOHERENCE

In order to accurately model any physical system such as, e.g., cesium atomic spins, we must include the effects of decoherence due to interaction with the environment. We perform simulations for the specific case of the cold atom system including photon scattering which results in nonunitary evolution. We model the evolution of the density operator ρ of the system using a master equation of the form

$$\frac{d\rho}{dt} = \frac{i}{\hbar}[H,\rho] + \sum_q \left[D_q \rho D_q^\dagger - \frac{1}{2}\{D_q^\dagger D_q, \rho\} \right]. \quad (20)$$

The jump operators $D_q = \epsilon_q \cdot \mathbf{d}_{ge}$ describe spontaneous emission from the excited states [38]. The excited states are adiabatically eliminated by assuming that the ground state populations change slowly compared to the excited states and the coherences. The excited state populations are thus effectively slaved to the ground state populations to give a net evolution only in terms of the ground state manifold $F=4$. Furthermore, any population which is pumped into the $F=3$ ground state is treated as a loss and ignored in the subsequent dynamics. This is possible if atoms in the $F=3$ manifold are not reexcited and therefore do not participate further in the observed dynamics. This model has provided accurate simulations of the physical system in recent experiments [20,26,27].

A. Effect of decoherence on entanglement

Figure 9 shows the simulated evolution [Eq. (20)] of the entropy $S(t)$ including decoherence for the three initial states analyzed in Fig. 2. Comparing the unitary evolution of Figs. 2(a)–2(c) to the nonunitary evolution due to decoherence in Figs. 9(a)–9(c), we see that the qualitative features are the same. The initial states in the regular regimes give rise to quasiperiodic motion, which is missing in the chaotic regime. Thus the signatures of chaos discussed in the previous section are also evident in the open system dynamics. However, although the signatures of chaos are preserved, there is an overall gradual increase in the linear entropy in the open system dynamics. Eventually all initial states will lead to maximum linear entropy. This is because the atoms are getting entangled with the environment via photon scattering. Thus the linear entropy no longer quantifies the $1:k$ entanglement of a single qubit (electron) with the rest (nucleus). Instead it quantifies the total entanglement of the electron with both the system and the environment. As the system becomes more entangled with the environment, there is an overall increase in entropy towards its maximum value of 0.5. The reason that the signatures of chaos seen in Fig. 2 remain robust to the effect of decoherence is because the photon scattering acts collectively on all the qubits and hence does not completely destroy the entanglement dynamics between the identical qubits interacting symmetrically via the kicked top Hamiltonian. Thus all the qubits get more entangled with the environment leading to an overall increase in the single qubit linear entropy, but the signatures of chaos arising from the internal dynamics within the system do not get completely destroyed until the system is maximally entangled with the environment.

In order to verify the collective effect of decoherence on the system, we compute the negativity as given by Eq. (15). Unlike the entropy S, the negativity N does give us a valid

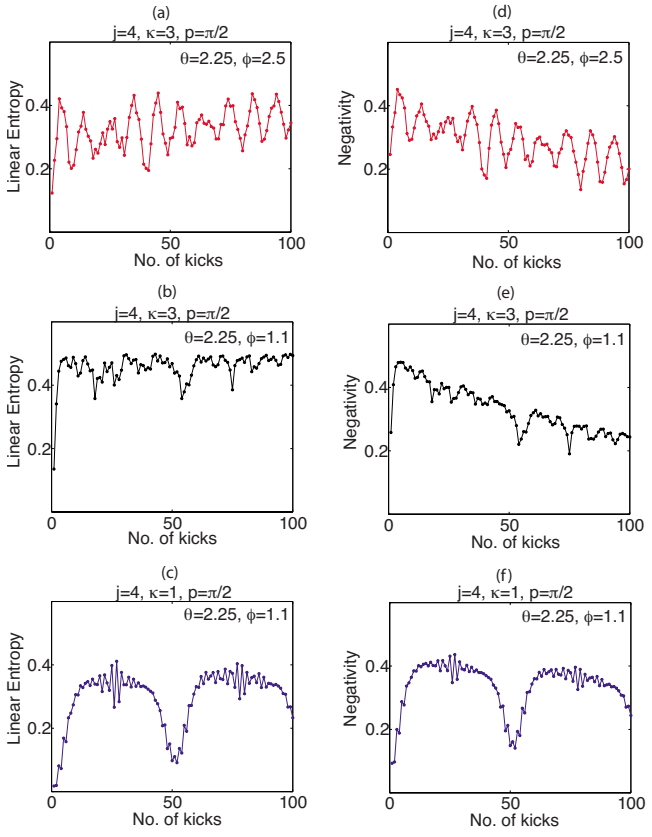

FIG. 9. (Color online) Evolution of the linear entropy S [(a)–(c)] and the negativity N [(d)–(f)] in the presence of decoherence (photon scattering) for initial spin coherent states $|\theta,\phi\rangle$ centered in regular versus chaotic regimes of the classical phase space. For comparison, the three initial states considered are picked to be the same as those in Fig. 2. See the text for details.

measure of $1:k$ entanglement for an overall mixed state resulting from tracing out the environment. Figures 9(d)–9(f) show the evolution of the negativity for the initial states considered in Fig. 2. We see that there is an overall decrease in the negativity but the quasiperiodic behavior in the regular regimes and the irregular dynamics in the chaotic regime exactly match the evolution of the entropy S in Figs. 9(a)–9(c). This confirms that the total spin state collectively gets more entangled with the environment, and accordingly the total $1:k$ entanglement within the system decreases. However, because decoherence acts collectively on the *total* spin system, the signatures of chaos caused by the interactions *within* the system are not completely destroyed and persist well beyond the scattering time. As described in Sec. III B, larger values of κ come at the cost of a higher photon scattering rate and thus a faster overall decoherence rate as seen in Fig. 9.

Although negativity has the advantage that it is a valid measure of entanglement for mixed states, it presents a disadvantage for experiments when compared to the linear entropy. This is because, in order to study negativity dynamics in an experiment, the total (nuclear+electron) state must be tomographically reconstructed. This is experimentally more challenging than measuring the linear entropy via measurements of $\langle F_\alpha \rangle$ [Eq. (9)]. Hence, in actual experiments, it may

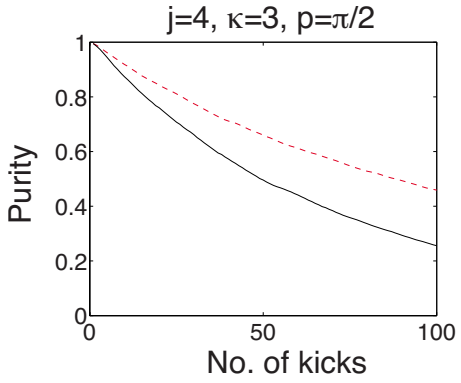

FIG. 10. (Color online) Purity decay (decoherence) of the overall spin state for different initial conditions with fixed $\kappa=3$, $p=\pi/2$. The decoherence rate is slower for an initial spin coherent state centered on a regular island with $|\theta=2.25,\phi=2.5\rangle$ (dashed) compared to an initial spin coherent state centered in the chaotic sea with $|\theta=2.25,\phi=1.1\rangle$ (solid), although the photon scattering rate is the same for both cases.

be more convenient only to measure the linear entropy S. Our comparison of the negativity and the linear entropy (Fig. 9) then clarifies that the decoherence only causes an overall decrease in the entanglement between electron and nuclear spin. Thus the linear entropy dynamics can be used to identify signatures of chaos in the entanglement between electron and nuclear spin even in the presence of decoherence. Furthermore, since the decoherence only causes an overall decrease in entanglement in both the regular and chaotic regimes, the time averaged entanglement will still be lower in the regular regions than in the chaotic regions as seen in the unitary evolution of Fig. 4. Signatures of chaos in the time averaged dynamics should thus be possible to observe in the experiment.

B. Effect of chaos on decoherence rate

In addition to examining the entanglement within the spin system, we can also analyze the entanglement of the total spin state with the environment due to photon scattering. We set the intensity, detuning, and Larmor frequency to obtain $\kappa=3$ and $p=\pi/2$. We then compare the decoherence rates of a spin coherent state centered on the regular island at $\theta=2.25$, $\phi=2.5$ and a spin coherent state centered in the chaotic sea at $\theta=2.25$ and $\phi=1.1$. Since the experimental parameters are the same for both cases, the scattering rate γ_s is also the same. However, despite the scattering rate being constant, we find that the decoherence rate is faster for the state initiated in the chaotic sea relative to the state starting on the regular island. In Fig. 10, we plot the purity of the overall state as a function of time. The purity decay is a measure of the decoherence and shows that the decoherence rate is faster for a state in the chaotic sea than for a state on a regular island. We have observed this increased rate of decoherence for states in a chaotic sea for other values of κ and p as well, indicating that chaos generally acts to increase the decoherence rate of the system.

The increase in the decoherence rate in the chaotic regime can be understood by examining the Lindblad terms in the

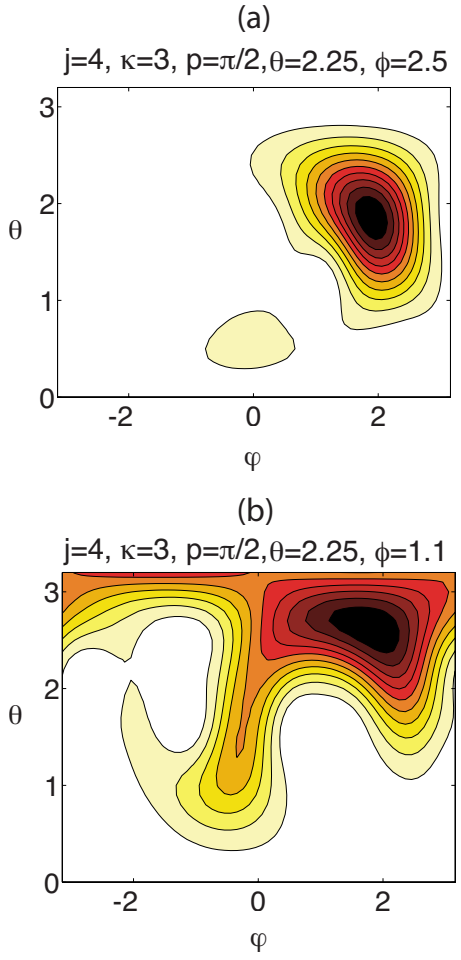

FIG. 11. (Color online) Husimi distributions after 50 kicks for the initial states considered in Fig. 10, with $\kappa=3$, $p=\pi/2$. Solid lines are contours of equiprobability distribution, and darker regions indicate larger probability. The initial spin coherent state centered on a regular island (a) with $|\theta=2.25,\phi=2.5\rangle$ remains closer to a robust spin coherent state, whereas the initial spin coherent state centered in the chaotic sea with $|\theta=2.25,\phi=1.1\rangle$ spreads quickly, leading to a delocalized state with net larger spontaneous emission and hence larger decoherence. θ,ϕ are plotted in units of radians.

master equation of Eq. (20) more carefully. The populations in the excited states which determine the spontaneous emission rate, depend on the ground state populations. Therefore we look at the evolution of the ground state populations in the regular versus chaotic regimes. Figure 11 shows the Husimi distributions after 50 kicks for the two initial spin coherent states centered in the regular island and chaotic sea. The initial state on a regular island remains close to a more robust spin coherent state. The Lindblad jump operators for this state lead to a net lower spontaneous emission rate. For the initial state in the chaotic sea, the dynamics causes the population distribution to quickly lose any symmetry and diverge from a coherent state. The spontaneous emission for such a state leads to a net larger decoherence rate.

Our results support the arguments originally formulated by Zurek and Paz [14,15] showing that chaos can affect the rate of decoherence. Their analysis showed that in the chaotic regime, the rate of decoherence is determined by the classical Lypunov exponents. Since the original work, further numerical and analytical studies have explored this idea to develop a more detailed picture of the quantitative connections between chaos and the decoherence rate in different regimes of coupling strength and chaoticity parameter [22–24]. The relevance of our work is that we consider a realistic and accurate decoherence model for an actual physical system very deeply in the quantum regime and verify the predictions obtained from semiclassical theories and more abstract decoherence models. In future work we plan to perform more detailed studies of the time scales for decoherence in this system.

VII. CONCLUSION

In summary, we have presented an analysis of entanglement and decoherence in the kicked top in a quantum regime of relevance to proposed experiments with cold cesium atoms. We have shown that $1:k$ entanglement can be easily measured from the mean angular momentum vector, and signatures of chaos are evident in the dynamics of entanglement in this quantum regime. The regular versus chaotic behavior can be understood by examining the decomposition of the initial state into regular and chaotic eigenstates of the Floquet operator. Our studies of dynamics in the deeply quantum regime shed new light on quantum-classical correspondence by showing that clear signatures of classical chaos can be identified far away from the semiclassical regime. Our results demonstrate truly quantum chaos in the sense that the system operates in a deeply quantum regime and signatures of chaos are observed in quantum properties such as entanglement and decoherence.

Our simulations of the realistic system of cold atoms undergoing decoherence due to photon scattering reveal that decoherence reduces the $1:k$ entanglement but does not erase the signatures of chaos. Furthermore, we have shown that chaos can enhance the overall decoherence rate, or entanglement of the system with the environment. This shows that whereas chaos can be helpful for generating entanglement within the system, it can have negative effects by rapidly causing decoherence.

We have thus shown a means for performing the first experimental studies of entanglement in a chaotic system, identified signatures of chaos in entanglement in a quantum regime that previous theoretical studies have not investigated, and extended the previous theoretical analysis to this quantum regime. Furthermore, we have demonstrated the collective effect of decoherence on the entanglement, and identified and explained signatures of chaos in the decoherence rate using a realistic model of decoherence. The cold atom experiments would be the first to realize the kicked top and study entanglement in a chaotic system. They would be

a stepping stone towards developing a robust set of experimental techniques for quantum control of multiqubit systems. An effort to implement the experiments decribed here is currently under way.

ACKNOWLEDGMENTS

We thank I. H. Deutsch for discussions and insights. S.G. was supported by an NSERC Discovery grant.

[1] E. Ott, *Chaos in Dynamical Systems* (Cambridge University Press, Cambridge, 2002).
[2] B. Georgeot and D. L. Shepelyansky, Phys. Rev. E **62**, 3504 (2000); **62**, 6366 (2000).
[3] M. A. Nielsen and I. L. Chuang, *Quantum Computation and Quantum Information* (Cambridge University Press, Cambridge, 2000).
[4] T. Prosen, J. Phys. A, special Issue on Quantum Information (to be published).
[5] K. Furuya, M. C. Nemes, and G. Q. Pellegrino, Phys. Rev. Lett. **80**, 5524 (1998); P. A. Miller and S. Sarkar, Phys. Rev. E **60**, 1542 (1999).
[6] A. Lakshminarayan, Phys. Rev. E **64**, 036207 (2001); J. N. Bandyopadhyay and A. Lakshminarayan, Phys. Rev. Lett. **89**, 060402 (2002); S. Bettelli and D. L. Shepelyansky, Phys. Rev. A **67**, 054303 (2003); A. J. Scott and C. M. Caves, J. Phys. A **36**, 9553 (2003).
[7] A. Tanaka, H. Fujisaki, and T. Miyadera, Phys. Rev. E **66**, 045201(R) (2002); H. Fujisaki, T. Miyadera, and A. Tanaka, *ibid.* **67**, 066201 (2003); G. Stamatiou and D. P. K. Ghikas, Phys. Lett. A **368**, 206 (2007).
[8] M. Znidaric and T. Prosen, J. Phys. A **36**, 2463 (2002); T. Prosen and T. Seligman, *ibid.* **35**, 4707 (2002).
[9] X. G. Wang, S. Ghose, B. C. Sanders, and B. Hu, Phys. Rev. E **70**, 016217 (2004).
[10] S. Ghose and B. C. Sanders, Phys. Rev. A **70**, 062315 (2004).
[11] A. Lahiri, e-print arXiv:quant-ph/0302029.
[12] P. Jacquod, Phys. Rev. Lett. **92**, 150403 (2004).
[13] J. Karthik, A. Sharma, and A. Lakshminarayan, Phys. Rev. A **75**, 022304 (2007); M. S. Santhanam, V. B. Sheorey, and A. Lakshminarayan, Phys. Rev. E **77**, 026213 (2008); W. G. Brown, L. F. Santos, D. J. Starling, and L. Viola, *ibid.* **77**, 021106 (2008); A. J. Scott *et al.*, J. Phys. A **39**, 13405 (2008).
[14] W. H. Zurek and J. P. Paz, Phys. Rev. Lett. **72**, 2508 (1994).
[15] W. H. Zurek and J. P. Paz, Physica D **83**, 300 (1995).
[16] H. Frahm and H. J. Mikeska, Z. Phys. B: Condens. Matter **60**, 117 (1985).
[17] F. Haake, M. Kus, and R. Scharf, Z. Phys. B: Condens. Matter **65**, 381 (1987).
[18] C. Cohen-Tannoudji, B. Diu, and F. Laloe, *Quantum Mechanics* (Wiley Interscience, Paris, 2006).
[19] G. A. Smith, S. Chaudhury, and P. S. Jessen, J. Opt. B: Quantum Semiclassical Opt. **5**, 323 (2003).
[20] G. A. Smith, S. Chaudhury, A. Silberfarb, I. H. Deutsch, and P. S. Jessen, Phys. Rev. Lett. **93**, 163602 (2004).
[21] G. S. Agarwal, Phys. Rev. A **24**, 2889 (1981).
[22] A. K. Pattanayak, Phys. Rev. Lett. **83**, 4526 (1999); D. Monteoliva and J. P. Paz, *ibid.* **85**, 3373 (2000).
[23] T. Gorin and H. Seligman, J. Opt. B: Quantum Semiclassical Opt. **4**, S386 (2002).
[24] C. Petitjean and P. Jacquod, Phys. Rev. Lett. **97**, 194103 (2006).
[25] Y. S. Weinstein and L. Viola, Europhys. Lett. **76**, 746 (2006).
[26] G. A. Smith, A. Silberfarb, I. H. Deutsch, and P. S. Jessen, Phys. Rev. Lett. **97**, 180403 (2006).
[27] S. Chaudhury, S. Merkel, T. Herr, A. Silberfarb, I. H. Deutsch, and P. S. Jessen, Phys. Rev. Lett. **99**, 163002 (2007).
[28] I. H. Deutsch and P. S. Jessen, Phys. Rev. A **57**, 1972 (1998); I. H. Deutsch *et al.*, J. Opt. B: Quantum Semiclassical Opt. **2**, 633 (2000).
[29] J. M. Geremia, J. K. Stockton, and H. Mabuchi, Phys. Rev. A **73**, 042112 (2006).
[30] J. T. Verdeyen, *Laser Electronics* (Prentice Hall, Englewood Cliffs, 1995).
[31] F. T. Arrechi *et al.*, Phys. Rev. A **6**, 2211 (1972).
[32] G. Vidal and R. F. Werner, Phys. Rev. A **65**, 032314 (2002).
[33] J. Lee, M. S. Kim, Y. J. Park, and S. Lee, J. Mod. Opt. **47**, 2151 (2000); M. B. Plenio, Phys. Rev. Lett. **95**, 090503 (2005).
[34] M. Horodecki, P. Horodecki, and R. Horodecki, Phys. Rev. Lett. **80**, 5239 (1998).
[35] A. Peres, Phys. Rev. Lett. **77**, 1413 (1996).
[36] V. I. Oseledec, Trans. Mosc. Math. Soc. **19**, 197 (1968); J. P. Eckmann and D. Ruelle, Rev. Mod. Phys. **57**, 617 (1985).
[37] G. Benettin, L. Galgani, and J.-M. Strelcyn, Phys. Rev. A **14**, 2338 (1976); G. Benettin, L. Galgani, A. Giorgilli, and J.-M. Strelcyn, Meccanica **15**, 9 (1980); A. Wolf, J. B. Swift, H. L. Swinney, and J. A. Vastano, Physica D **16**, 285 (1985).
[38] A. Silberfarb, Ph.D. thesis, University of New Mexico, 2006 (unpublished).